Symmetry-forbidden x-ray Raman scattering induced by a strong infrared-laser field

Ji-Cai Liu,[1,2,*] Yasen Velkov,[1] Zilvinas Rinkevicius,[1] Hans Ågren,[1] and Faris Gel'mukhanov[1]
[1]*Department of Theoretical Chemistry, School of Biotechnology, Royal Institute of Technology, S-106 91 Stockholm, Sweden*
[2]*College of Physics and Electronics, Shandong Normal University, 250014 Jinan, China*
(Received 8 February 2008; revised manuscript received 12 March 2008; published 3 April 2008)

Resonant inelastic x-ray scattering accompanied by core-hole hopping induced by a strong infrared-laser field is studied for the nitrogen molecule. This process involves a strong laser-field-induced promotion of ungerade core holes created by a weak x-ray pulse to a gerade core level, which opens symmetry-forbidden scattering channels and gives rise to new features in the x-ray scattering spectrum. The core-hole hopping within the short lifetime of the core-excited state required for observation of the described process can be achieved at moderate intensities of the infrared field ($\sim 10^{12}$ W/cm^2) because of the large transition dipole moment between the relevant core levels. The dynamics of resonant inelastic x-ray scattering assisted by change of core-hole parity is studied in detail versus the intensity, detuning, phase, and duration of the incident infrared-laser and x-ray pulses.

DOI: 10.1103/PhysRevA.77.043405 PACS number(s): 34.50.Rk, 33.20.Rm, 34.50.Gb, 41.60.Cr

I. INTRODUCTION

The monitoring of nuclear and electronic motions in real time is one of the main aims of ultrafast optical and x-ray spectroscopies [1]. The typical approaches for recording molecular motion in real time rely on pump-probe schemes, and new opportunities for time-resolved multicolor pump-probe x-ray experiments [2,3] have emerged in recent years with the development of advanced harmonic generation techniques as well as x-ray free-electron lasers. Despite considerable progress in pump-probe spectroscopy in the optical region, a similar development in the x-ray region has been lacking, and most x-ray measurements are currently performed with continuous-wave light sources or with long pulses. A few real x-ray measurements with femtosecond resolution form an exception to this trend. They employ x-ray pump-probe schemes based on probing x-ray absorption or photoionization of optically or infrared (ir) excited molecules [3–8]. One remarkable example of application of time-resolved pump-probe spectroscopy in the x-ray region is the attosecond sampling of x-ray-induced electron wave packets [2,3]. However, mainstream application of x-ray pump-probe spectroscopy on femtosecond and shorter time scales still remains beyond the current technical capabilities, and new developments in experimental techniques, instrumentation for measurements, and theory are needed before spectroscopy of this kind becomes more widely applicable.

X-ray spectroscopy is a powerful tool for probing electronic structure, the nature of chemical bonding, and excitation dynamics. Relevant investigations have become popular owing to the recent development in synchrotron radiation and in experimental techniques. Conventional resonant inelastic x-ray scattering (RIXS) [9–11] is based on the resonant excitation of a core electron to an unoccupied molecular orbital (MO) followed by spontaneous decay of an electron from an occupied MO into the created core hole. Unlike the first-order x-ray absorption and emission processes, RIXS is a combination of x-ray absorption and emission events. RIXS associated with the dipole selection rules for each step provides a direct way to detect the symmetry of the core-excited states [10–13], which cannot be achieved by either nonresonant or nonradiative x-ray spectroscopy.

In this paper, we suggest and explore in detail a scheme of x-ray pump-probe spectroscopy–RIXS induced by core-hole hopping in a strong laser field. In solids and symmetric molecules, the core shell consists of few or many close-lying core levels. The small molecular orbital splitting of the core shell lying in the far-ir region (~ 0.1 eV) is comparable with the lifetime broadening Γ of the core-excited states of light atoms like carbon, nitrogen, or oxygen. Due to this circumstance it is rather difficult to resolve such small core-hole splittings [14–18] using x-ray photoelectron spectroscopy. However, RIXS in a strong laser field gives direct information about fine structure of core shells which is hidden in conventional spectroscopies by the large lifetime broadening. Indeed, the modern advances in strong-field laser physics make it possible to promote the short-living core hole into a core level of opposite parity by applying an ir- or optical-laser pulse. The laser-induced change of parity of the core hole opens symmetry-forbidden scattering channels and gives information about the fine structure of the core shell. The x-ray pump-probe experiment proposed here demonstrates that RIXS is a unique tool for probing the dynamics of Rabi flopping [19] of core holes induced by a laser field.

The paper is organized as follows. A physical picture of RIXS induced by core-hole hopping in a strong laser field is presented in Sec. II A. We outline in Sec. II B the basic theory. To give insight into the physics of RIXS in a strong laser field, we analyze the studied process using an analytical solution for rectangular pulses (Sec. II C). The general theory is exemplified for x-ray scattering of the N_2 molecule. The core-excited and final states of this molecule are discussed in Sec. III. The final expressions for the RIXS cross sections of fixed-in-space and randomly oriented molecules are derived in Sec. IV. Numerical simulations are discussed in Sec. V. Our findings are summarized in Sec. VII.

*Corresponding author. jicai@theochem.kth.se

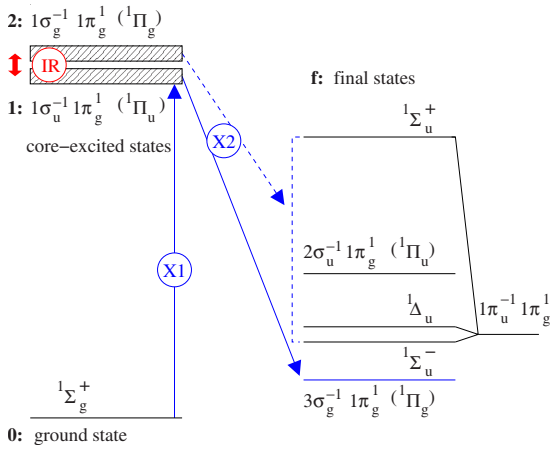

FIG. 1. (Color online) Scheme of RIXS transitions in the ir-laser field.

II. THEORY

A. Physical picture of x-ray scattering in a strong laser field

The ground-state electronic configuration of N_2 is

$$(1\sigma_g)^2,(1\sigma_u)^2,(2\sigma_g)^2,(2\sigma_u)^2,(1\pi_u)^4,(3\sigma_g)^2, \quad X\ ^1\Sigma_g^+.$$

The lowest unoccupied molecular orbital (LUMO) in N_2 is the $1\pi_g$ orbital. The spacing between the core orbitals $1\sigma_g$ and $1\sigma_u$ is comparable with the lifetime broadening of the x-ray transition. This means that core holes can be created in both levels $1\sigma_g$ and $1\sigma_u$. However, the resonant excitation creates core holes only in one of these orbitals. Indeed, when the frequency of the incident x-ray radiation ω_{X1} is tuned near resonance with the transition to the LUMO, $1\sigma_{g,u} \rightarrow 1\pi_g$, only the transition $1\sigma_u \rightarrow 1\pi_g$ is allowed due to the dipole selection rules. This means that the radiative decay channel is allowed only from the gerade occupied molecular orbital [10,11], $3\sigma_g \rightarrow 1\sigma_u$, as has been confirmed by experiment [13]. The picture changes qualitatively when the molecule is exposed to a strong ir laser tuned in resonance with the $1\sigma_u \rightarrow 1\sigma_g$ core transition. The laser field promotes the core hole into the core level of opposite parity and opens thereby the symmetry-forbidden fluorescence channels $(1\pi_u, 2\sigma_u) \rightarrow 1\sigma_g$.

B. Amplitude equations and RIXS cross section

The energy level scheme of the RIXS transitions in the N_2 molecule is shown in Fig. 1. There are two qualitatively different RIXS channels in the ir-laser field: (1) the symmetry-allowed channel $^1\Sigma_g^+ \rightarrow (1\sigma_u^{-1}1\pi_g^1)\ ^1\Pi_u \rightarrow f$ with one gerade final state $f=(3\sigma_g^{-1}1\pi_g^1)\ ^1\Pi_g$ and (2) the symmetry-forbidden ones $^1\Sigma_g^+ \rightarrow (1\sigma_g^{-1}1\pi_g^1)\ ^1\Pi_g \rightarrow f$ with four ungerade final states $f=(2\sigma_u^{-1}1\pi_g^1)\ ^1\Pi_u$, $(1\pi_u^{-1}1\pi_g^1)\ ^1\Sigma_u^-$, $^1\Delta_u$, and $^1\Sigma_u^+$.

When the final state is fixed, it is sufficient to consider a four-level molecule which interacts with the low-frequency pump field (L), the high-frequency incident x-ray radiation (X1), and the scattered x-ray radiation (X2):

$$\mathcal{E}_\alpha(t) = \mathbf{e}_\alpha E_\alpha(t)\cos(\omega_\alpha t + \varphi_\alpha), \quad \alpha = \mathrm{L,X1,X2}. \tag{1}$$

These fields mix the ground (ψ_0), two core-excited (ψ_1 and ψ_2), and final (ψ_f) states (Fig. 1) with the energies $E_i=\hbar\omega_i$: $\psi=\Sigma_i a_i\psi_i$. The SI system of units is used here. In the interaction picture, the amplitudes a_i obey the equations

$$\dot{a}_i + \Gamma_i a_i = -\imath \sum_j e^{\imath\omega_{ij}t} U_{ij} a_j, \quad \omega_{ij} = (E_i - E_j)/\hbar, \tag{2}$$

$$U_{ij} = -\frac{1}{\hbar}\mathbf{d}_{ij}\cdot[\mathcal{E}_{\mathrm{X1}}(t) + \mathcal{E}_{\mathrm{X2}}(t) + \mathcal{E}_{\mathrm{L}}(t)],$$

where it is supposed that the lifetime broadenings of the two core-excited states are the same, $\Gamma_1=\Gamma_2=\Gamma$. We assume that the weak incident x-ray field does not change the ground-state population, $a_0 \approx 1$, and that the weak scattered spontaneous x-ray field does not affect the population of the core-excited states. It is natural to treat both of the weak x-ray fields in the rotating wave approximation (RWA), in contrast to the strong laser field which is taken into account explicitly. This allows us to simplify Eqs. (2),

$$\dot{a}_1 + \Gamma a_1 = \frac{\imath}{2} e^{\imath(\omega_{10}-\omega_{\mathrm{X1}})t - \imath\varphi_{\mathrm{X1}}} G_{10}^{\mathrm{X1}} + \imath e^{-\imath\omega_{21}t} G_{12}^{L} \cos(\omega_{\mathrm{L}}t + \varphi_{\mathrm{L}}) a_2,$$

$$\dot{a}_2 + \Gamma a_2 = \imath e^{\imath\omega_{21}t} \cos(\omega_{\mathrm{L}}t + \varphi_{\mathrm{L}}) G_{21}^{\mathrm{L}} a_1, \quad G_{20}^{\mathrm{X1}} = 0,$$

$$\dot{a}_f + \Gamma_f a_f = \frac{\imath}{2}(e^{\imath(\omega_{\mathrm{X2}}-\omega_{1f})t} G_{f1}^{\mathrm{X2}} a_1 + e^{\imath(\omega_{\mathrm{X2}}-\omega_{2f})t} G_{f2}^{\mathrm{X2}} a_2). \tag{3}$$

Here $G_{ij}^{\alpha}=(\mathbf{e}_\alpha\cdot\mathbf{d}_{ij})E_\alpha/\hbar$ are Rabi frequencies of the x-ray absorption and emission transitions (α=X1,X2) and of the laser transitions between the core-excited states (α=L). We have taken into account in Eq. (3) that $G_{20}^{\mathrm{X1}}=0$ because the transition $0 \rightarrow 2$ is dipole forbidden. It is worth noting that, according to the dipole selection rules, for each scattering channel, one of the Rabi frequencies $(G_{f1}^{\mathrm{X2}}, G_{f2}^{\mathrm{X2}})$ is equal to zero,

$$G_{f1}^{X2} = 0, \quad f = u; \quad G_{f2}^{X2} = 0, \quad f = g, \tag{4}$$

because the core-excited states have opposite parities: the upper state ψ_2 is gerade, while the lower state ψ_1 is ungerade (see Fig. 1).

The RIXS cross section is calculated through the final-state population $\rho_f=|a_f|^2$,

$$\sigma = \sum_f \sigma_f, \quad \sigma_f = \int_{-\infty}^{\infty} \rho_f(t)dt. \tag{5}$$

The constant prefactor is neglected at the right-hand side of this equation.

The time of the Rabi flopping $1/G_{12}^L$ must be faster than the lifetime of the core-excited state $1/\Gamma$ in order to promote significant population transfer from the symmetry-allowed core-excited state ψ_1 to the symmetry-forbidden state ψ_2. This happens when the intensity of the laser field exceeds the threshold value

$$I_L > I_{\text{th}}, \quad I_{\text{th}} = 2c\epsilon_0\left(\frac{\hbar\Gamma}{d_{12}}\right)^2. \tag{6}$$

A simple calculation gives a reasonable value of the threshold intensity $I_{\text{th}} \sim 10^{12}$ W/cm^2, attributed to the large dipole moment ($d_{12} \approx 2.6379$ D) of the charge-transfer transition between the ungerade $\psi_1 \equiv |1\sigma_u^{-1}1\pi_g^1\rangle$ and the gerade $\psi_2 \equiv |1\sigma_g^{-1}1\pi_g^1\rangle$ core holes [20],

$$\mathbf{d}_{12} = e\langle 1\sigma_u|\mathbf{r}|1\sigma_g\rangle = \frac{e}{2}\int \mathbf{r}[1s^2(\mathbf{r}-\mathbf{R}_1) - 1s^2(\mathbf{r}-\mathbf{R}_2)]d\mathbf{r}$$

$$\approx \frac{e\mathbf{R}}{2}. \tag{7}$$

Here $\mathbf{R}$ is the interatomic radius vector, which is assumed to be along the z axis.

C. Core-hole promotion by a rectangular laser pulse

To get insight into the dynamics of the population of core-excited states, it is instructive to write down the solution of Eq. (3) for overlapping rectangular x-ray and laser pulses with $\Gamma_f = 0$. In this section, the rotating wave approximation is also used for the ir-laser pulse by assuming in Eq. (3) that

$$e^{\mp \iota\omega_{21}t}\cos(\omega_L t) \approx \frac{1}{2}e^{\pm\iota(\omega_L-\omega_{21})t}, \quad \varphi_{X1} = \varphi_L = 0. \tag{8}$$

Though the RWA breaks down in strong laser fields (see Sec. V), this approximation is useful for qualitative analysis. The RWA solution of Eqs. (3) and (8) inside the pulses ($0 \le t \le \tau$) is straightforward,

$$\begin{pmatrix} a_1 \\ a_2 \end{pmatrix} = \frac{\iota G_{X1}e^{-\iota\Omega_{X1}t}}{4\Delta}\left[\begin{pmatrix} \Omega_L + \Delta \\ -G_{21}^L e^{-\iota\Omega_L t}\end{pmatrix} \times\left(\frac{1-e^{-\Gamma t}e^{\iota(\Omega_{X1}+\Omega_L/2-\Delta/2)t}}{\Gamma - \iota(\Omega_{X1}+\Omega_L/2-\Delta/2)}\right) + \begin{pmatrix} \Delta - \Omega_L \\ G_{21}^L e^{-\iota\Omega_L t}\end{pmatrix} \times\left(\frac{1-e^{-\Gamma t}e^{\iota(\Omega_{X1}+\Omega_L/2+\Delta/2)t}}{\Gamma - \iota(\Omega_{X1}+\Omega_L/2+\Delta/2)}\right)\right], \quad 0 \le t \le \tau, \tag{9}$$

where $\Omega_{X1} \equiv \omega_{X1} - \omega_{10}$ and $\Omega_L \equiv \omega_L - \omega_{21}$ are, respectively, the detuning energies of the incident x-ray and laser fields from the resonances, and τ is the duration of the rectangular pulses. One can see that the x-ray absorption resonance experiences a Rabi splitting

$$\Delta = \sqrt{(G_{21}^L)^2 + \Omega_L^2}, \tag{10}$$

caused by the laser-induced transitions between the core-excited states. To see the role of the laser field, let us write the ratio of populations for $\Omega_L = \Omega_{X1} = 0$ and $\Gamma t \gg 1$,

$$\frac{\rho_2}{\rho_1} = \left(\frac{G_{12}^L/2}{\Gamma}\right)^2 = \frac{I_L}{I_{\text{th}}}. \tag{11}$$

When the intensity of the laser field is high enough, $G_{12}^L = 2\Gamma$, the symmetry-forbidden core-excited state ψ_2 has the same population as the state ψ_1. The laser-induced population of state ψ_2 depends resonantly on the frequency of the laser field $\rho_2 \propto (G_{12}^L)^2/[(\omega_L - \omega_{21})^2 + (G_{21}^L)^2]$, where the Rabi frequency results in a field broadening.

The laser-induced population of the symmetry-forbidden core-excited state ψ_2 and the Rabi splitting of both core-excited states affect the RIXS profile (5) strongly, as one can see from the expression (9) of the final-state amplitude,

$$a_f = \frac{\iota}{2}\int_{-\infty}^{t}[e^{\iota(\omega_{X2}-\omega_{1f})t_1}G_{f1}^{X2}a_1(t_1) + e^{\iota(\omega_{X2}-\omega_{2f})t_1}G_{f2}^{X2}a_2(t_1)]e^{-\Gamma_f(t-t_1)}dt_1. \tag{12}$$

III. CORE-EXCITED AND FINAL STATES

The N_2 molecule has two doubly degenerate core-excited states (see Fig. 1),

$$\Psi_c^{x,y}(^1\Pi_u) = |1\sigma_u^{-1}1\pi_g^1(x,y)\rangle, \quad \Psi_c^{x,y}(^1\Pi_g) = |1\sigma_g^{-1}1\pi_g^1(x,y)\rangle, \tag{13}$$

and five final states, of which one gerade state is obtained by promotion of an electron from the highest occupied molecular orbital (HOMO) ($3\sigma_g$) to the LUMO ($1\pi_g$),

$$\Psi^{x,y}(^1\Pi_g) = |3\sigma_g^{-1}1\pi_g^1(x,y)\rangle, \tag{14}$$

and four ungerade states are generated by electron excitation from HOMO-1 ($1\pi_u$) or HOMO-2 ($2\sigma_u$) to the LUMO ($1\pi_g$),

$$\Psi^{x,y}(^1\Pi_u) = |2\sigma_u^{-1}1\pi_g^1(x,y)\rangle,$$

$$\Psi(^1\Delta_u)_{1,2}, \quad \Psi(^1\Sigma_u^+), \quad \Psi(^1\Sigma_u^-): \quad 1\pi_u^{-1}1\pi_g^1. \tag{15}$$

The states $\Psi(^1\Pi_g)$, $\Psi(^1\Pi_u)$, and $\Psi(^1\Delta_u)$ are doubly degenerate. The origin of the splitting of the $|1\pi_u^{-1}1\pi_g^1\rangle$ final states is the difference of the electron-hole interactions $1\pi_u^{-1}(x) - 1\pi_g^1(x)$ and $1\pi_u^{-1}(x) - 1\pi_g^1(y)$. To compute the transition dipole moments we need the wave functions of the final states,

$$\Psi(^1\Delta_u)_1 = \frac{1}{\sqrt{2}}[|1\pi_u(x)1\pi_g(y)\rangle - |1\pi_u(y)1\pi_g(x)\rangle],$$

$$\Psi(^1\Delta_u)_2 = \frac{1}{\sqrt{2}}[|1\pi_u(y)1\pi_g(y)\rangle + |1\pi_u(x)1\pi_g(x)\rangle],$$

$$\Psi(^1\Sigma_u^+) = \frac{1}{\sqrt{2}}[|1\pi_u(y)1\pi_g(y)\rangle - |1\pi_u(x)1\pi_g(x)\rangle],$$

$$\Psi(^1\Sigma_u^-) = \frac{1}{\sqrt{2}}[|1\pi_u(x)1\pi_g(y)\rangle + |1\pi_u(y)1\pi_g(x)\rangle]. \tag{16}$$

We have the following nonzero transition dipole moments of x-ray absorption and emission transitions:

$$\langle\Psi_c^{x,y}(^1\Pi_u)|\mathbf{r}|0\rangle = d_{c0}\cdot(\hat{\mathbf{x}},\hat{\mathbf{y}}),$$

$$\langle\Psi_c^{x,y}(^1\Pi_{g,u})|\mathbf{r}|\Psi^{x,y}(^1\Pi_{u,g})\rangle = d_{cf}\cdot\hat{\mathbf{z}}, \quad f = {}^1\Pi_u, {}^1\Pi_g,$$

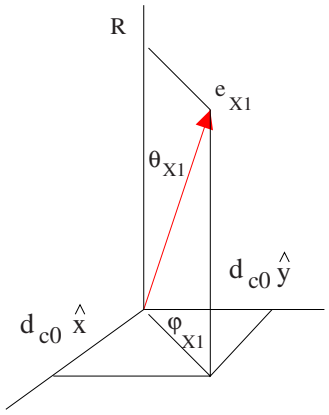

FIG. 2. (Color online) Angles between the polarization vector $\mathbf{e}_{X1}$ of the incident x-ray pulse and the transition dipole moments of core excitation $1\sigma_u \rightarrow 1\pi_g$ in the molecular frame.

$$\langle \Psi_c^{x,y}(^1\Pi_g)|\mathbf{r}|f\rangle = d_{cf}\cdot(\hat{\mathbf{x}},\hat{\mathbf{y}}), \quad f=(^1\Delta_u)_{1,2}, {}^1\Sigma_u^+, {}^1\Sigma_u^-. \tag{17}$$

Here the unit vectors $(\hat{\mathbf{x}},\hat{\mathbf{y}},\hat{\mathbf{z}})$ show the directions of the transition dipole moments in the molecular frame (see Fig. 2). It is worth noting that the final states $f=(^1\Delta_u)_{1,2}, {}^1\Sigma_u^+, {}^1\Sigma_u^-$ have the same d_{cf}. The absolute values of the dipole moments (17) are collected in Table I.

IV. AVERAGING OVER MOLECULAR ORIENTATIONS

The RIXS depends on the orientations of the polarization vectors relative to the transition dipole moments through the Rabi frequencies. It is convenient to extract this orientational dependence from the Rabi frequencies of x-ray transitions,

$$G_{10}^{X1}(\mathbf{e}_{X1}\cdot\hat{\mathbf{d}}_{10}), \quad G_{fc}^{X2}(\mathbf{e}_{X2}\cdot\hat{\mathbf{d}}_{fc}). \tag{18}$$

Here $\hat{\mathbf{d}}=\mathbf{d}/d$ is the unit vector along $\mathbf{d}$. Now the Rabi frequencies

$$G_{10}^{X1}=E_{X1}d_{10}/\hbar, \quad G_{fc}^{X2}=E_{X2}d_{fc}/\hbar \tag{19}$$

do not depend on the molecular orientation. Let us extract the orientational dependence from the amplitudes

$$a_{1,2}=\tilde{a}_{1,2}(\mathbf{e}_{X1}\cdot\hat{\mathbf{d}}_{10}), \quad a_f=\tilde{a}_f(\mathbf{e}_{X1}\cdot\hat{\mathbf{d}}_{10})(\mathbf{e}_{X2}\cdot\hat{\mathbf{d}}_{fc}). \tag{20}$$

It is easy to see that the new amplitudes $\tilde{a}_{1,2}$ and $\tilde{a}_f$ obey the same equation as Eq. (3) except that the Rabi frequencies G_{10}^{X1} and G_{fc}^{X2} are defined for parallel orientations between the polarization vectors and the corresponding transition dipole moments [see Eq. (19)]. Now Eq. (3) depends only on the angle $\theta=\angle\,\mathbf{e}_L,\mathbf{R}$ between the molecular axis and the polarization vector of the laser field.

A. Cross section for fixed-in-space molecules

According to Eq. (20), $\rho_f=|\tilde{a}_f|^2(\mathbf{e}_{X1}\cdot\hat{\mathbf{d}}_{10})^2(\mathbf{e}_{X2}\cdot\hat{\mathbf{d}}_{fc})^2$. Taking this into account and the dipole moments of core excitation and emission transitions as expressed in (17), we get the following RIXS cross section (5) for fixed-in-space molecules:

$$\sigma(\theta)=\sin^2\theta_{X1}\{\cos^2\theta_{X2}[\sigma_{3\sigma_g}(\theta)+\sigma_{2\sigma_u}(\theta)] + \frac{1}{2}\sin^2\theta_{X2}[\sigma_{1\pi_u}^{^1\Sigma_u^-}(\theta)+\sigma_{1\pi_u}^{^1\Sigma_u^+}(\theta)+2\sigma_{1\pi_u}^{^1\Delta_u}(\theta)]\}, \tag{21}$$

summed over all final states. Here $\theta_{X1}=\angle\,\mathbf{e}_{X1},\mathbf{R}$ and $\theta_{X2}=\angle\,\mathbf{e}_{X2},\mathbf{R}$. The partial RIXS cross sections

TABLE I. Core-excited and final states of N_2. ω_{cf} are the resonant emission frequencies of the symmetry-allowed emission transitions $|1\rangle=|c(u)\rangle\rightarrow|f(g)\rangle$ and $|2\rangle=|c(g)\rangle\rightarrow|f(u)\rangle$ for $\Omega_L=\Omega_{X1}=0$. Asterisks mark parameters that are used in simulations. The dipole moments d_{cf} and d_{c0} are normalized to 1 for the strongest transition. $\Gamma=0.0575$ eV [18].

Final state	ω_{f0} (eV) Expt.[a] (theory)	ω_{cf}^* (eV) Expt.	d_{cf} Expt.[b] (theory*)
$^1\Pi_g\ \|3\sigma_g^{-1}1\pi_g^1\rangle$	9.31 (9.38)	392.1[b]	1 (1)
$^1\Sigma_u^-\ \|1\pi_u^{-1}1\pi_g^1\rangle$	9.92 (9.99)	391.587[a,b]	0.559 (0.625)
$^1\Delta_u\ \|1\pi_u^{-1}1\pi_g^1\rangle$	10.27 (10.43)	391.237[a,b]	0.559 (0.625)
$^1\Pi_u\ \|2\sigma_u^{-1}1\pi_g^1\rangle$	12.78 (13.25)	388.727[a,b]	0.433 (0.426)
$^1\Sigma_u^+\ \|1\pi_u^{-1}1\pi_g^1\rangle$	14.35 (16.37)	387.157[a,b]	0.559 (0.625)
Core-excited state	-	ω_{c0}^* (eV) (expt.)	d_{c0}
$^1\Pi_u\ \|1\sigma_u^{-1}1\pi_g^1\rangle$	-	400.88[b]	1
$^1\Pi_g\ \|1\sigma_g^{-1}1\pi_g^1\rangle$	-	400.977[b,c]	0
ir transition	ω_{21}^* (eV) (expt.)	-	d_{21}^* (theory)
$1\sigma_u\rightarrow1\sigma_g$	0.097[c]	-	2.6379 D

[a]Experimental data from Refs. [24,25].
[b]Experimental data from Ref. [13].
[c]Experimental data from Ref. [18].

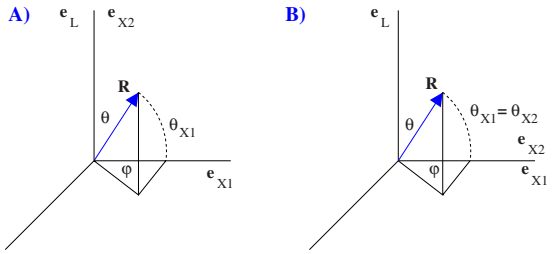

FIG. 3. (Color online) Scheme of two different geometries. (a) $\theta=\theta_{X2}$, $(\mathbf{e}_L \| \mathbf{e}_{X2}) \perp \mathbf{e}_{X1}$; (b) $\theta_{X1}=\theta_{X2}$, $\mathbf{e}_L \perp (\mathbf{e}_{X2} \| \mathbf{e}_{X1})$.

$$\sigma_{3\sigma_g}, \quad \sigma_{2\sigma_u}, \quad \sigma_{1\pi_u}^{1\Sigma_u^-}, \quad \sigma_{1\pi_u}^{1\Sigma_u^+}, \quad \sigma_{1\pi_u}^{1\Delta_u} \tag{22}$$

correspond to the decay transitions with a degeneracy factor equal to 1. The subscript marks the occupied MO from which the emission transition occurs. The partial cross sections σ_f (22) are calculated using Eq. (5) for $\mathbf{e}_{X1} \| \mathbf{d}_{10}$ and $\mathbf{e}_{X2} \| \mathbf{d}_{fc}$ as is described in the first paragraph of this section (Sec. IV).

B. X-ray Raman scattering from randomly oriented molecules

We consider two geometries of the RIXS (Fig. 3).

Geometry A [Fig. 3(a)]. The polarizations of the incident laser pulse and of the emitted x-ray radiation are parallel to each other and they are perpendicular to that of the incident x-ray pulse:

$$(\mathbf{e}_L \| \mathbf{e}_{X2}) \perp \mathbf{e}_{X1}, \quad \theta = \theta_{X2}. \tag{23}$$

In this case $\cos\theta_{X1}=\sin\theta\cos\varphi$. Averaging of the RIXS cross section (21) over the rotation of the molecular axis around $\mathbf{e}_L$ ($\overline{\cos^2\varphi}=1/2$) results in the following expression:

$$\sigma(\theta) = \frac{1}{2}\left(1-\frac{1}{2}\sin^2\theta\right)\{2\cos^2\theta[\sigma_{3\sigma_g}(\theta)+\sigma_{2\sigma_u}(\theta)] + \sin^2\theta[\sigma_{1\pi_u}^{1\Sigma_u^-}(\theta)+\sigma_{1\pi_u}^{1\Sigma_u^+}(\theta)+2\sigma_{1\pi_u}^{1\Delta_u}(\theta)]\}. \tag{24}$$

Geometry B [Fig. 3(b)]. The polarizations of the two x-ray fields are parallel to each other and they are perpendicular to that of the ir-laser pulse:

$$\mathbf{e}_L \perp (\mathbf{e}_{X2} \| \mathbf{e}_{X1}), \quad \theta_{X1} = \theta_{X2}. \tag{25}$$

Now $\cos\theta_{X2}=\cos\theta_{X1}=\sin\theta\cos\varphi$. The RIXS cross section (21) averaged over φ reads

$$\sigma(\theta) = \frac{1}{2}\left(1-\frac{1}{2}\sin^2\theta\right)\left\{\sin^2\theta[\sigma_{3\sigma_g}(\theta)+\sigma_{2\sigma_u}(\theta)] + \left(1-\frac{1}{2}\sin^2\theta\right)[\sigma_{1\pi_u}^{1\Sigma_u^-}(\theta)+\sigma_{1\pi_u}^{1\Sigma_u^+}(\theta)+2\sigma_{1\pi_u}^{1\Delta_u}(\theta)]\right\}. \tag{26}$$

The orientational averaging over rotations of the molecular axis relative to the polarization vector of the ir-laser field $\mathbf{e}_L$, namely, the averaging over θ, is performed numerically using the equation

$$\sigma = \frac{1}{2}\int_0^\pi \sigma(\theta)\sin\theta\, d\theta. \tag{27}$$

V. COMPUTATIONAL ASPECTS

After extracting the orientational factors (20), the amplitude equations (3) are numerically solved for the amplitudes $\tilde{a}_1$, $\tilde{a}_2$, and $\tilde{a}_f$ with the angle-dependent Rabi frequency of the core-hole transition

$$G_{12}^L = \frac{E_L d_{12}}{\hbar}\cos\theta. \tag{28}$$

The partial RIXS cross sections (22) are then evaluated using Eq. (5). Finally, the orientational averaging is performed with Eqs. (24)–(27) following the procedure outlined in Sec. IV.

The temporal shapes of the incident x-ray and ir-laser pulses are modeled by Gaussians with the same peak position t_0,

$$E_\alpha(t) = E_\alpha^{(0)}\exp\{-[(t-t_0)/\tau_\alpha]^2 \ln 2/2\}, \quad \alpha = X1, L, \tag{29}$$

where τ_α is the half width at half maximum (HWHM) of the intensity profile of the pulse. The emission transitions are triggered by weak time-independent spontaneous noise, and due to this we put $E_{X2}=1$.

The values of the excitation energies and of the transition dipole moments relevant to the present simulations are collected in Table I. The results of our *ab initio* calculations are compared with available experimental data in Table I. The data marked with asterisks are used as input spectroscopic data in the numerical simulations, and the small lifetime broadening of the final states is neglected. The theoretical values for the transition energies ω_{ij} and the dipole moments d_{ij} are obtained at the equilibrium geometry of the nitrogen molecule using second-order N-electron valence-state perturbation theory (NEVPT2) [21] and the single configuration interaction (SCI) method, respectively. The NEVPT2 calculations are carried out employing an active space consisting of the valence orbitals of interest, namely, $2\sigma_g$, $2\sigma_u$, $1\pi_u$, $3\sigma_g$, and $1\pi_g$, in the augmented correlation consistent polarized valence 5-ζ (aug-cc-pV5Z) basis set [22]. The transition dipole moments are calculated using the SCI method in the triple-ζ valence augmented with $(2p,2df)$ polarization function [TZV $(2p,2df)$] basis set [23]. From the results presented in Table I one can see that our theoretical NEVPT2 transition energies ω_{f0} of the $0\rightarrow f$ transitions are in good agreement with the experimental ones [24,25]. The resonant frequencies ω_{cf} of the x-ray decay transitions have been recalculated using the experimental peak position of the $^1\Pi_u|1\sigma_u^{-1}1\pi_g^1\rangle \rightarrow {}^1\Pi_g|3\sigma_g^{-1}1\pi_g^1\rangle$ symmetry-allowed x-ray Raman resonance [13] and the absorption data [25] for ω_{f0} (Table I). The theoretical values of d_{cf} are close to those extracted from off-resonant x-ray fluorescence measurements [13].

VI. DISCUSSION OF NUMERICAL SIMULATIONS

The RIXS spectra calculated with the two geometries A [Fig. 3(a)] and B [Fig. 3(b)] are shown in Fig. 4 for different intensities of the ir field. One can see that, when the ir-laser

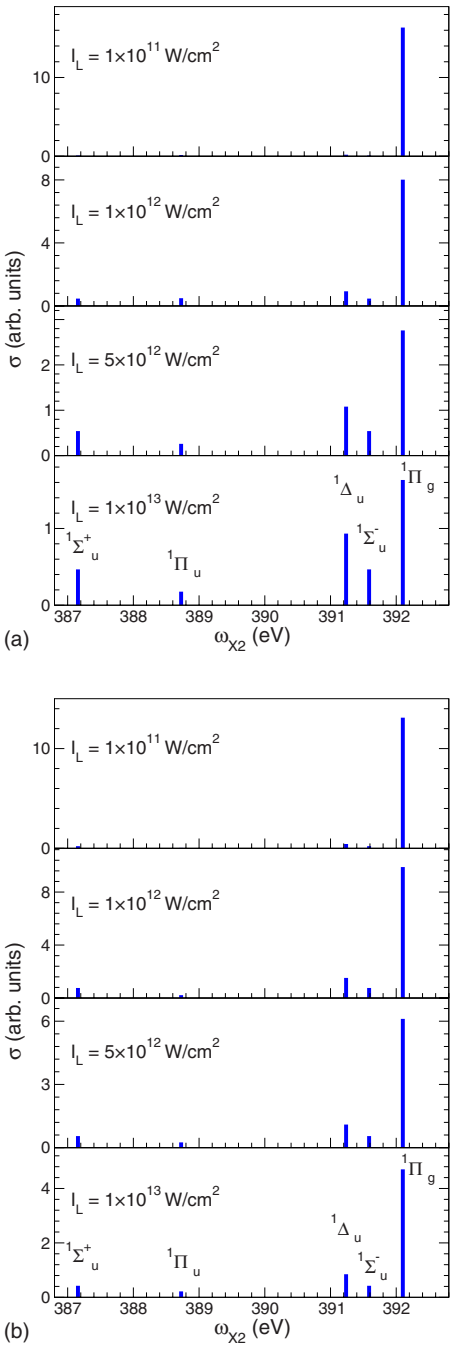

FIG. 4. (Color online) RIXS spectra for different peak intensities I_L of the ir field. The symmetry-forbidden channels are opened when I_L exceeds the threshold intensity $\approx 10^{12}$ W/cm^2. $\tau_X = \tau_L = 1$ ps. $\Omega_{X1} \equiv \omega_{X1} - \omega_{10} = 0$. $\Omega_L \equiv \omega_L - \omega_{21} = 0$. $\varphi_{X1} = \varphi_L = 0$. (a) Geometry A; (b) geometry B.

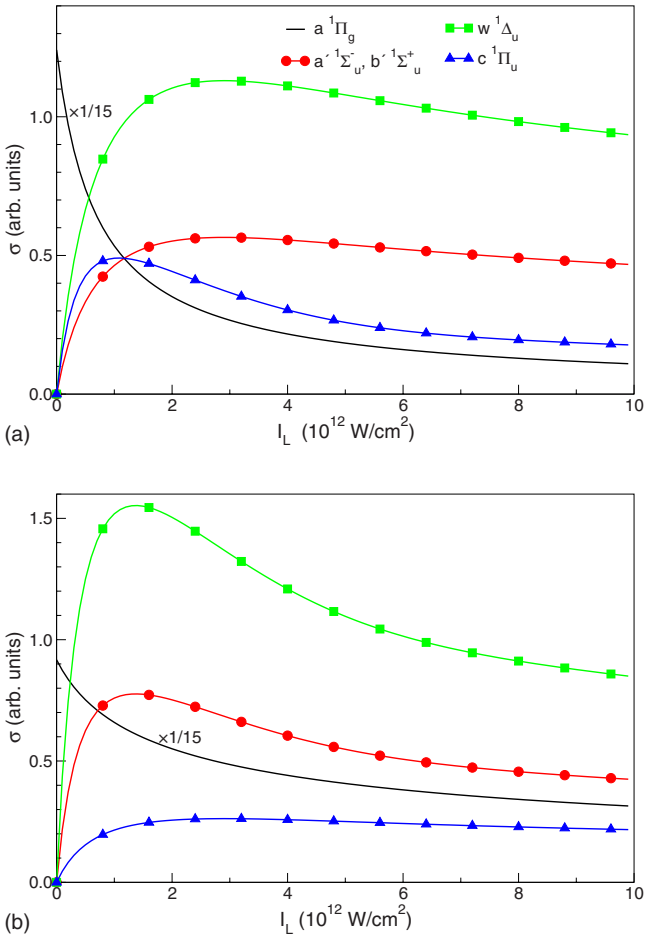

FIG. 5. (Color online) Partial RIXS cross sections versus the intensity of the ir field. $\tau_{X1} = \tau_L = 1$ ps. The symmetry-allowed scattering channel ($a\ ^1\Pi_g$) is shown by the solid line. $\Omega_{X1} = \Omega_L = 0$. $\varphi_{X1} = \varphi_L = 0$. (a) Geometry A; (b) geometry B.

pulse is weak, only the symmetry-allowed channel is observed. However, when the intensity of the ir pulse exceeds the threshold value (6) $\approx 10^{12}$ W/cm^2, the symmetry-forbidden channels are opened. When the Rabi frequency of the ir transition exceeds the lifetime broadening of the core-excited states, the ir field mixes, to a large extent, the ungerade ($^1\Pi_u$) and the gerade ($^1\Pi_g$) core-excited states. Therefore, the emission transitions from the gerade core-excited state to the ungerade final states are detected. Comparing Figs. 4(a) and 4(b), one can also see that the RIXS spectrum depends on the relative polarization directions of the x-ray and ir-laser fields.

The partial RIXS cross sections of different decay channels are presented as a function of the intensity of the incident ir pulse in Fig. 5. As is expected, the partial RIXS cross sections of the symmetry-forbidden channels start to grow from zero when I_L increases. The maximum values are reached when the Rabi frequency of the ir transition is comparable with or larger than the lifetime broadening of the core-excited states ($\hbar G_{12}^L \approx 0.15$ eV for $I_L = 10^{12}$ W/cm^2 and $\theta = 0$). However, the cross sections begin to decrease for higher ir-pump levels. The suppression of the partial cross sections for higher intensities is due to the Rabi splitting of the core-excited states caused by the strong ir field. This can be illustrated from the analytical RWA solutions (9) of the amplitude equations for the overlapped rectangular incident pulses. The Rabi splitting (10), which is different for different instants and θ, leads to a broadening of the x-ray absorption profile and suppresses the resonant x-ray absorption probability. In contrast, the symmetry-allowed peak ($^1\Pi_g$) decreases monotonically when the ir field intensity increases (Fig. 5). The reason for this is twofold. The first one is the

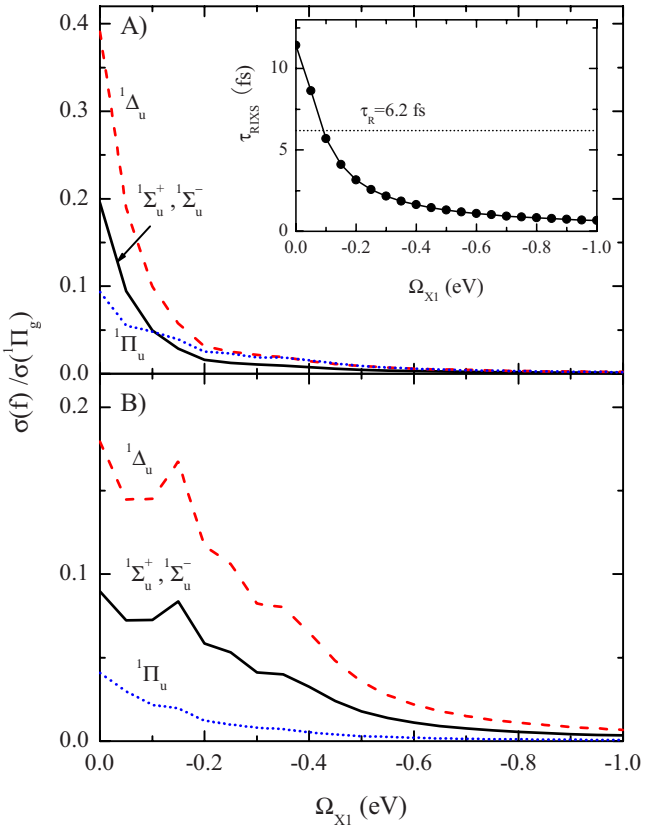

FIG. 6. (Color online) Cross section of the forbidden RIXS channels relative to that of the symmetry-allowed $^1\Pi_g$ channel versus the detuning Ω_{X1}. The inset shows the dependence of the RIXS duration τ_{RIXS} on the detuning Ω_{X1}. $\tau_X=\tau_L=1$ ps. $\Omega_L=0$. The peak intensity of the ir-laser pulse $I_L=5.0\times10^{12}$ W/cm^2. $\varphi_{X1}=\varphi_L=0$. (a) Geometry A; (b) geometry B.

depopulation of the intermediate symmetry-allowed core-excited state $^1\Pi_u$ due to the ir transition to the upper core-excited state $^1\Pi_g$ (Fig. 1). This mechanism dominates until $I_L\approx2\times10^{12}$ W/cm^2. The second reason is the above-mentioned Rabi splitting which starts to be important for higher intensities.

It is known that the effective duration of the RIXS process, $\tau_{\mathrm{RIXS}}=1/\sqrt{\Omega_{X1}^2+\Gamma^2}$, depends strongly on the detuning of the incident x-ray radiation from the resonant absorption transition [11,26]. The dynamical process can be controlled by varying the duration of RIXS through tuning the frequency of the incident x-ray pulse. On the other hand, the time of Rabi flopping $\tau_R=\pi/G_{21}^L$ determines the efficiency of the core-hole hopping between the ungerade and gerade core levels. Hence, the effect studied here depends on the competition of the time of Rabi flopping between the core holes τ_R and the duration of the x-ray pulse τ_{X1} or the scattering duration τ_{RIXS}. The influence of the detuning Ω_{X1} on the ratio of the cross section of the forbidden RIXS channel relative to that of the symmetry-allowed one is shown in Fig. 6. One can see that the symmetry-forbidden channels are strongly suppressed with large detuning Ω_{X1} since τ_{RIXS} is shorter than τ_R (inset of Fig. 6). In this case, most of the ungerade core holes have already decayed to the final state through the symmetry-allowed channel before they have the opportunity to be excited to the gerade core level.

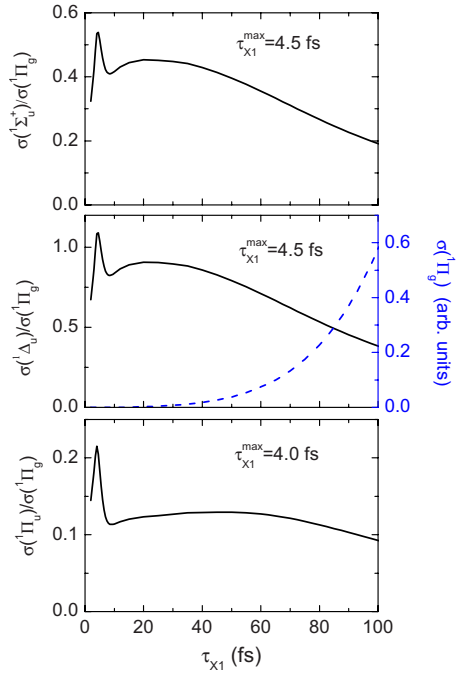

FIG. 7. (Color online) Relative cross sections of forbidden peaks $\sigma(f)/\sigma(^1\Pi_g)$ detected with geometry A versus duration of the incident x-ray pulse. $\tau_{X1}^{\max}$ is the value of τ_{X1} when $\sigma(f)/\sigma(^1\Pi_g)$ is a maximum. The dashed line shows the cross section of the symmetry-allowed channel as a function of the HWHM of the incident x-ray pulse. $\tau_L=100$ fs. $\Omega_{X1}=\Omega_L=0$. The peak intensity of the ir-laser pulse $I_L=5.0\times10^{12}$ W/cm^2. $\varphi_{X1}=\varphi_L=0$.

The shortening of the incident x-ray pulse τ_{X1} is expected to suppress the symmetry-forbidden RIXS channels. In fact, this is not true and the opposite trend is observed (Fig. 7). The relative peak intensities of the symmetry-forbidden channels $\sigma(f)/\sigma(^1\Pi_g)$ become stronger for shorter duration of the x-ray pulse, although the absolute intensity of each decay channel is decreased (dashed line in Fig. 7). When the relative intensity of the symmetry-forbidden channel takes the maximum value, the duration of the x-ray pulse has the same order of magnitude (4.5 fs) as the time of Rabi flopping of the core holes. The shortening of the incident x-ray pulse (Fig. 8) results in another effect, namely, additional spectral features compared with the case of a long pulse (Fig. 4, $I_L=5\times10^{12}$ W/cm^2). The reason for this is the interplay of the two resonant features of the scattering process [10,11,27] $\omega_{X2}=\omega_{X1}-\omega_{f0}$ and $\omega_{X2}=\omega_{cf}$,

$$\sigma\propto\frac{1}{(\omega_{X2}-\omega_{cf})^2+\Gamma^2}\Phi(\omega_{X2}-(\omega_{X1}-\omega_{f0}),\gamma). \quad (30)$$

To give a qualitative explanation of the extra spectral features seen in Fig. 8, the cross section (30) is written here for a three-level molecule. The spectral function of the incident x-ray beam is very narrow $\gamma\sim1/\tau_{X1}\ll\Gamma$, when the duration of the incident pulse τ_{X1} is longer than $1/\Gamma$. In this case, the RIXS spectral profile displays the Raman peaks $\omega_{X2}=\omega_{X1}-\omega_{f0}$ which do not depend on the energies of the core-excited states (Fig. 4). The picture changes qualitatively when the x-ray pulse is short $\gamma\sim1/\tau_{X1}\gtrsim\Gamma$. Now both Ra-

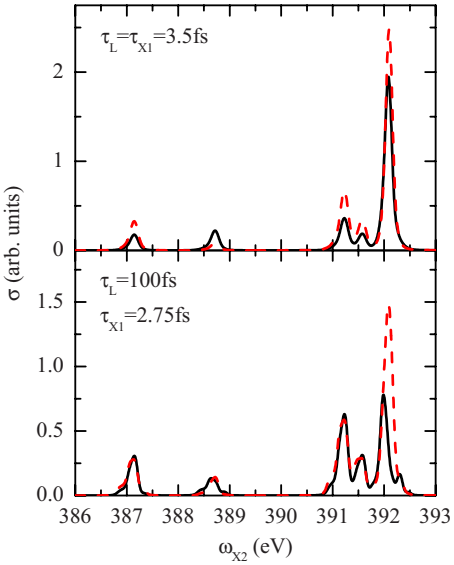

FIG. 8. (Color online) RIXS spectra for short incident x-ray and ir-laser pulses. Solid line for geometry A, dashed line for geometry B. $\Omega_{X1}=\Omega_L=0$. $I_L=5.0\times10^{12}$ W/cm^2. $\varphi_{X1}=\varphi_L=0$.

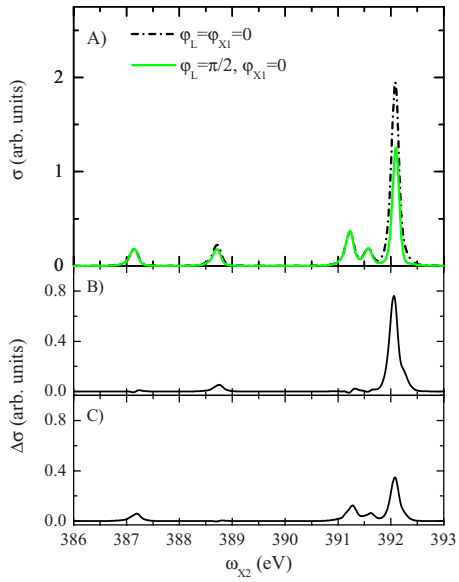

FIG. 9. (Color online) Effect of the phase on RIXS spectra for short incident x-ray and ir-laser pulses with $\tau_L=\tau_{X1}=3.5$ fs. (a) compares the RIXS profiles (geometry A) for $\varphi_{X1}=0$, $\varphi_L=\pi/2$ (solid line) and $\varphi_{X1}=\varphi_L=0$ (dash-dotted line). (b) and (c) show the differences of the RIXS cross sections $\Delta\sigma=\sigma(\varphi_L=0)-\sigma(\varphi_L=\pi/2)$ for the geometries A and B, respectively ($\varphi_{X1}=0$). The other parameters are the same as in Fig. 8.

man ($\omega_{X2}=\omega_{X1}-\omega_{f0}$) and non-Raman ($\omega_{X2}=\omega_{cf}$) peaks are seen in RIXS. The Rabi splitting of the core-excited states $c=1,2$ [see Eq. (9)] explains the appearance of the extra peaks in the RIXS profile shown in Fig. 8.

Previous calculations were performed for zero phases of the weak x-ray and strong ir fields, $\varphi_{X1}=\varphi_L=0$. It is natural to expect a phase sensitivity of the RIXS when the pulses are short [28]. To check the role of the phases, we calculated the RIXS profiles for different phases of short x-ray and ir pulses. The simulations shown in Fig. 9 display the phase sensitivity of the RIXS. To shed light on the origin of the observed phase effect, we calculated the spectra for two different sets of phases ($\varphi_{X1}=0$, $\varphi_L=\pi/2$) and ($\varphi_{X1}=\pi/4$, $\varphi_L=\pi/2$) with the same phase of the ir field. These two sets of phases give exactly the same profiles. This means that the RIXS profile is sensitive only to the absolute phase φ_L of the few-cycle strong ir field and does not depend on the phase of the weak x-ray pulse φ_{X1}. One can see that the role of the phase is stronger for the geometry A, where the phase affects mainly the symmetry-allowed peak.

We have investigated RIXS in a strong ir field under core excitation into an unoccupied $1\pi_g$ molecular orbital. It is worth noting that the studied effect takes place also when the x-ray photon is tuned above the ionization threshold near the shape resonance. This expectation is based on both theoretical [9] and experimental [13] investigations of ordinary RIXS under core excitation near the σ_u shape resonance in the N_2 molecule.

A few words about the possibility for experimental observation of RIXS accompanied by laser-induced hopping of core holes are in order. The observation can be done with different molecules like N_2, O_2, or C_2H_2. The main requirement is the intensity of the laser pulse. It should be large enough to make the time of Rabi flopping of core holes comparable with the lifetime of the core-excited state. Calculations show that a far-ir laser with peak intensity about 10^{12} W/cm^2 is needed for the N_2 molecule. Other molecules (O_2 and C_2H_2) need approximately the same intensity due to the similar values of the charge-transfer transition dipole moments and lifetimes of the core holes. The effect discussed can be observed in a rather wide range of pulse durations ($\gtrsim1$ fs). In principle, one can use a continuous-wave laser as well. An appropriate laser system could be a terawatt (TW) CO_2 laser [29]. The Accelerator Test Facility (ATF) at Brookhaven National Laboratory is constructing a tabletop TW picosecond CO_2 laser system which will be synchronized with the electron bunches [30] and will in our view provide an excellent tool for the observation of RIXS induced by core-hole flopping.

VII. SUMMARY

We have investigated theoretically a scheme for RIXS accompanied by core-hole hopping induced by a strong laser field. The dynamics of RIXS has been exemplified in detail with the N_2 molecule. This scheme of RIXS provides a powerful tool for probing the dynamics of Rabi flopping of short-living core holes. A weak x-ray pulse is used to create the core hole by exciting an electron from the lowest ungerade core molecular orbital to the unoccupied gerade molecular orbital. Meanwhile, a synchronized strong ir-laser pulse drives the core holes from the ungerade to the gerade core-excited states, and opens the symmetry-forbidden RIXS channels. Therefore, symmetry-forbidden spectral components are observed in the RIXS spectrum. The effective four-level model is used to describe the RIXS process. In the amplitude equations, the rotating wave approximation is ap-

plied to both the incident and the scattered x-ray radiation, while the strong laser field is treated strictly. Expressions for the RIXS cross sections for both fixed-in-space and randomly oriented molecules are derived. The RIXS spectrum depends on the relative polarization directions of the x-ray and ir-laser fields. Two different scattering geometries are used to investigate the RIXS. It is found that the symmetry-forbidden components of the RIXS spectrum become observable when the Rabi frequency of the ir-laser transition is comparable with the lifetime broadening of the core-excited states. On the other hand, the Rabi splitting of the core-excited states induced by the stronger ir pulse results in a broadening of the x-ray absorption profile and decreases the RIXS probability. The strength of the symmetry-forbidden channel strongly depends on the competition of the time of Rabi flopping between the core holes and the effective RIXS duration or the duration of the x-ray pulse. The shortening of the incident pulses gives rise to a broadening of the RIXS spectrum. Moreover, the resonant positions are shifted due to the interplay of the Raman and non-Raman components of the scattering process. When the incident pulses are short, the RIXS profile is sensitive to the absolute phase of the few-cycle strong ir field and is independent of the phase of the weak x-ray pulse. It is argued that these findings can be verified by available laboratory equipment.

ACKNOWLEDGMENTS

We acknowledge support from the Swedish Research Council (VR), Carl Tryggers Stiftelse (CTS) foundation, and National Basic Research Program for China Grant No. 2006CB806000. This work was also supported by a grant from the Swedish Infrastructure Committee (SNIC) for the project "Multiphysics Modeling of Molecular Materials," No. SNIC 023/07-18.

[1] A. H. Zewail, J. Phys. Chem. A **104**, 5660 (2000).
[2] M. Drescher, M. Hentschel, R. Klenberger, M. Ulberacker, V. Yakovlev, A. Scrinzl, Th. Westerwalbesloh, U. Kleineberg, U. Heinzmann, and F. Krausz, Nature (London) **419**, 803 (2002).
[3] C. Bressler and M. Chergui, Chem. Rev. **104**, 1781 (2004).
[4] D. Cubaynes, M. Meyer, A. N. Grum-Grzhimailo, J.-M. Bizau, E. T. Kennedy, J. Bozek, M. Martins, S. Canton, B. Rude, N. Berrah, and F. J. Wuilleumier, Phys. Rev. Lett. **92**, 233002 (2004).
[5] T. Privalov, F. Gel'mukhanov, and H. Ågren, J. Electron Spectrosc. Relat. Phenom. **129**, 43 (2003).
[6] M. Meyer, D. Cubaynes, P. O'Keeffe, H. Luna, P. Yeates, E. T. Kennedy, J. T. Costello, P. Orr, R. Taïeb, A. Maquet, S. Düsterer, P. Radcliffe, H. Redlin, A. Azima, E. Plönjes, and J. Feldhaus, Phys. Rev. A **74**, 011401(R) (2006).
[7] J. Schulz, M. Tchaplyguine, T. Rander, H. Bergersen, A. Lindblad, G. Öhrwall, S. Svensson, S. Heinäsmäki, R. Sankari, S. Osmekhin, S. Aksela, and H. Aksela, Phys. Rev. A **72**, 032718 (2005).
[8] J. Schulz, S. Heinäsmäki, R. Sankari, T. Rander, A. Lindblad, H. Bergersen, G. Öhrwall, S. Svensson, E. Kukk, S. Aksela, and H. Aksela, Phys. Rev. A **74**, 012705 (2006).
[9] F. Gel'mukhanov and H. Ågren, J. Phys. B **29**, 2751 (1996).
[10] F. Gel'mukhanov and H. Ågren, Phys. Rev. A **49**, 4378 (1994).
[11] F. Gel'mukhanov and H. Ågren, Phys. Rep. **312**, 87 (1999).
[12] P. Glans, K. Gunnelin, P. Skytt, J.-H. Guo, N. Wassdahl, J. Nordgren, H. Ågren, F. Kh. Gel'mukhanov, T. Warwick, and E. Rotenberg, Phys. Rev. Lett. **76**, 2448 (1996).
[13] P. Glans, P. Skytt, K. Gunnelin, J.-H. Guo, and J. Nordgren, J. Electron Spectrosc. Relat. Phenom. **82**, 193 (1996).
[14] B. Kempgens, H. Köppel, A. Kivimäki, M. Neeb, L. S. Cederbaum, and A. M. Bradshaw, Phys. Rev. Lett. **79**, 3617 (1997).
[15] T. D. Thomas, N. Berrah, J. Bozek, T. X. Carroll, J. Hahne, T. Karlsen, E. Kukk, and L. J. Sæthre, Phys. Rev. Lett. **82**, 1120 (1999).
[16] U. Hergenhahn, O. Kugeler, A. Rüdel, E. E. Rennie, and A. M. Bradshaw, J. Phys. Chem. A **105**, 5704 (2001).
[17] K. Ueda, X.-J. Liu, G. Prümper, T. Lischke, T. Tanaka, M. Hoshino, H. Tanaka, I. Minkov, V. Kimberg, and F. Gel'mukhanov, Chem. Phys. **329**, 329 (2006).
[18] X.-J. Liu, G. Prümper, F. Gel'mukhanov, N. A. Cherepkov, H. Tanaka, and K. Ueda, J. Electron Spectrosc. Relat. Phenom. **156–158**, 73 (2007).
[19] T. Udem, Nature (London) **420**, 469 (2002).
[20] R. S. Mulliken, J. Chem. Phys. **7**, 14 (1939).
[21] C. Angeli, R. Cimiraglia, S. Evangelisti, T. Leininger, and J. P. Malrieu, J. Chem. Phys. **114**, 10252 (2001).
[22] T. H. Dunning, Jr., J. Chem. Phys. **90**, 1007 (1989).
[23] A. Schafer, C. Huber, and R. Ahlrichs, J. Chem. Phys. **100**, 5829 (1994).
[24] G. Huber and G. Herzberg, *Spectra of Diatomic Molecules* (Van Nostrand, Princeton, NJ, 1979).
[25] J. Oddershede, N. E. Grüner, and G. H. F. Diercksen, Chem. Phys. **97**, 303 (1985).
[26] F. Gel'mukhanov, P. Sałek, T. Privalov, and H. Ågren, Phys. Rev. A **59**, 380 (1999).
[27] F. Gel'mukhanov and H. Ågren, Phys. Lett. A **193**, 375 (1994).
[28] F. F. Guimarães, V. Kimberg, V. C. Felicíssimo, F. Gel'mukhanov, A. Cesar, and H. Ågren, Phys. Rev. A **72**, 012714 (2005).
[29] S. Ya. Tochitsky, R. Narang, C. Filip, C. E. Clayton, K. A. Marsh, and C. Joshi, Opt. Lett. **24**, 1717 (1999).
[30] www.bnl.gov/atf/core_ capabilities/co2sys.asp